JOURNAL OF MATERIALS SCIENCE 29 (1994) 5607–5611

Thermochemical modelling in CO_2 laser cutting of carbon steel

M. J. HSU, P. A. MOLIAN
Mechanical Engineering Department, Iowa State University, Ames, IA 50011, USA

A thermochemical heat transfer model in oxygen-assisted laser cutting of carbon steel has been developed in terms of the laser mode pattern, the power density, combustion reaction, kerf width and cutting speed. This model emphasizes the chemical combustion effect as well as the laser mode pattern, which are usually neglected by most existing laser cutting models. Good agreement was obtained between theoretical and experimental results, indicating that approximately 55–70% of the cutting energy is supplied by the combustion reaction of the steel with oxygen, which is consistent with experimental data obtained by other investigators.

Nomenclature

a	Focused laser beam diameter (m)
A	Absorptivity
ΔH	Heat of combustion ($J\,kg^{-1}$)
I	Power density ($W\,m^{-2}$)
k	Thermal diffusivity ($m^2\,s^{-1}$)
K	Thermal conductivity ($W\,m^{-1}\,K^{-1}$)
K_0	Modified Bessel function of the second kind and zeroth order
l	Workpiece thickness (m)
P	Laser power (W)
q	Heat rate (W)
q'	q/l: heat rate per unit length ($W\,m^{-1}$)
R	Half the kerf width (m)
s	$\frac{VR}{2\alpha}$: normalized cutting speed
T_{mp}	Melting temperature (K)
T_{rm}	Room temperature (K)
$T(x, y)$	Temperature at (x, y) (K)
V	Cutting speed ($m\,s^{-1}$)
W	$2R$: kerf width (m)
x, y, z	Cartesian co-ordinates
α	Thermal diffusivity ($m^2\,s^{-1}$)
δ	Average thickness of liquid melt film (m)
η	Combustion efficiency
θ, γ	Polar co-ordinates
ρ	Material density ($kg\,m^{-3}$)

1. Introduction

Industrial laser applications in manufacturing are primarily in the areas of machining and welding, which account for more than 70% of the total laser processing category in the USA [1]. In general, laser cutting with a coaxial oxygen jet significantly improves the cutting speed due to the combustion reaction between oxygen and the workpiece at the erosion cutting front (see Fig. 1). Laser cutting is a complex process and mathematical models have been developed by many investigators to describe the cutting phenomena [2–14]. Most of the existing laser cutting models neglect the combustion reaction and/or the energy distribution of the laser beam and often result in limited practical applications. Forbes [15] estimated that in oxygen-assisted laser cutting of steel, 70% of the cutting energy derived is from combustion. Kamalu and Steen [3] concluded that 60% of the cutting energy is supplied by combustion. On the other hand, Ivarson *et al.* [16] estimated that the oxidation process contributes 40% of the energy input to the cutting zone, and the laser provides the remaining 60%. Belforte [17] reported that high power lasers with a transmission electron microscope (TEM_{00}) (Gaussian) energy distribution can cut metals better and faster than a multi-mode laser beam.

Therefore, it is important to develop a theoretical model that describes the laser cutting process in terms of the combustion reaction and the energy distribution of the heat source. The basis of the present work originates from the effort by Bunting and Cornfield [18], who ignored the combustion effect and assumed a uniform power density heat source in their model. In the present analysis, the effects of combustion and the laser beam mode in the heat transfer analysis is included.

2. Experimental procedure

A continuous wave CO_2 laser (Spectra-Physics Model 820, maximum 2 kW output power) was used to cut AISI 1020 steel plates, with oxygen as assist gas. The thickness of the workpiece was varied from 1.27 to 12.7 mm. The laser was operated to 1500 W power. The laser beam exhibited a near TEM_{00} (Gaussian energy distribution) mode pattern. A nominal 127 mm zinc selenide (ZnSe) focusing lens was used to focus the laser beam to a spot size of 0.1 mm. The focal point

0022–2461

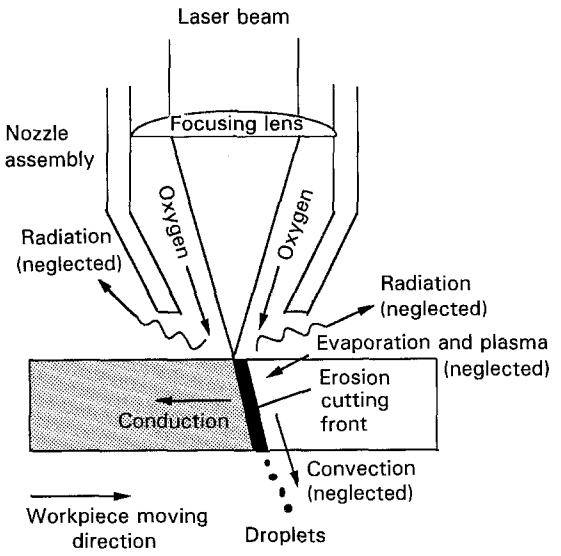

Figure 1 Schematic diagram of oxygen-assist laser cutting and heat transfer modes.

was set either on the surface of the workpiece in thin-section cutting or a distance equal to one-third the thickness from the surface in thick-section cutting (thickness > 6.3 mm). A convergent nozzle was used for oxygen gas flow and the reservoir oxygen pressure was varied from 0.069 to 0.276 MPa. The steel plates were mounted on a computer numerically controlled worktable and cut with the laser beam. The maximum cutting speed was recorded as the speed at which cutting through the thickness of workpiece became impossible. The experimental setup is illustrated in Fig. 1. Combustion products (such as droplets) were collected and analysed by X-ray diffraction (XRD) to determine the compounds and compositions. The kerf width was measured directly using a thickness gauge with an accuracy of 0.03 mm.

3. Theoretical modelling

3.1. Assumptions

The following assumptions are made to facilitate the theoretical modelling process:

1. A two-dimensional, moving heat source model for a slab is considered. The thermal gradient in the z direction (material thickness) is small compared to those in other directions if the material is relatively thin [19, 20].
2. Heat losses due to convection and radiation are negligible [21, 22].
3. Classical heat transfer theory is applicable to the laser heating process [3, 23].
4. Beam guiding and multiple reflection effects are ignored due to the high absorptivity in laser cutting of steel [24]. The increased absorptivity may be explained by plasma formation inside the cutting kerf.
5. No vaporization and associated latent heat is involved during laser cutting. This assumption may only be valid in cutting thick-section materials as evaporation occurs at the upper portion of the erosion cutting front.

3.2. Modelling

The governing differential equation for the two-dimensional steady state conduction heat transfer of a moving linear heat source at a velocity, V, in the x-direction is given by

$$\frac{\partial^2 T}{\partial x^2} + \frac{\partial^2 T}{\partial y^2} = \frac{V}{\alpha}\frac{\partial T}{\partial x} \tag{1}$$

subject to following boundary conditions

$$\text{(i)} \quad \frac{\partial T}{\partial x} \to 0 \text{ as } x \to \pm\infty$$

$$\text{(ii)} \quad \frac{\partial T}{\partial y} \to 0 \text{ as } y \to \pm\infty$$

$$\text{(iii)} \quad -2\pi r K \frac{\partial T}{\partial r} \to q' \text{ as } r \to 0, \text{ where } r = (x^2 + y^2)^{1/2}$$

The solution to the above equation was given by Carslaw and Jaegar [25].

$$\begin{aligned} T(x, y) &= T_{rm} + \frac{q}{2\pi lk}\exp(Vx/2\alpha) \\ &\quad \times \{K_0[V(x^2 + y^2)^{1/2}/2\alpha]\} \\ &= T_{rm} + \frac{q'}{2\pi k}\exp(Vx/2\alpha) \\ &\quad \times \{K_0[V(x^2 + y^2)^{1/2}/2\alpha]\} \end{aligned} \tag{2}$$

For a fixed point (x, y), the temperature rise due to polar co-ordinate linear heat source $q'(r, \theta)$ becomes

$$\begin{aligned} T(x, y) &= T_{rm} + \frac{q'}{2\pi k}\exp[V(x - r\cos\theta)/2\alpha] \\ &\quad \times K_0\{V[(x - r\cos\theta)^2 \\ &\quad + (y - r\sin\theta)^2]^{1/2}/2\alpha\} \end{aligned} \tag{3}$$

Consider now a focused laser beam as a moving heat source. Then, Equation 3 can be formulated as

$$\begin{aligned} T(x, y) &= T_{rm} + \frac{1}{2\pi lk}\int I_{total} r\,dr \\ &\quad \times \int \exp[V(x - r\cos\theta)/2\alpha] \\ &\quad \times K_0\{V[(x - r\cos\theta)^2 \\ &\quad + (y - r\sin\theta)^2]^{1/2}/2\alpha\}\,d\theta \end{aligned} \tag{4}$$

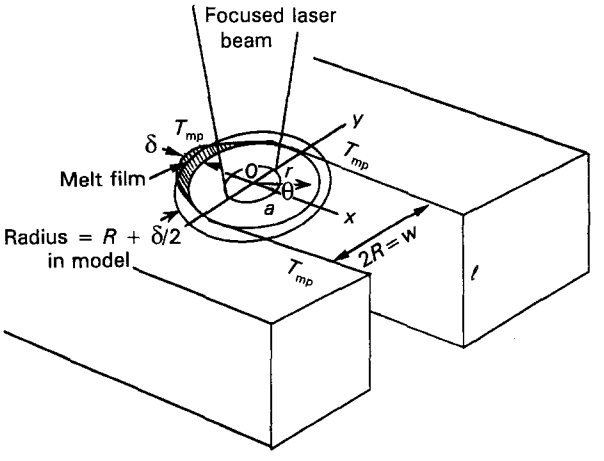

Figure 2 Laser cutting geometry.

where I_{total} is the total power density, which includes absorbed laser radiation and that derived from the related combustion reaction. Typically, isotherms of a moving heat source in a two-dimensional case show an elliptical shape with the long axis in the moving direction [19, 20]. By choosing $x = 0$ and $y = R$, the melting isotherm from Equation 4 coincides with the half of the kerf width, R. Then

$$T_{mp} = T(0,R) = T_{rm} + \frac{1}{2\pi lk}\int I_{total} r\,dr \times \int \exp(-Vr\cos\theta/2\alpha) \times K_0[V(R^2 - 2Rr\sin\theta + r^2)^{1/2}/2\alpha]d\theta \quad (5)$$

For a Gaussian mode (TEM_{00}) CO_2 laser beam, the power density, I_{laser}, is

$$I_{laser} = I_{max}\exp(-8r^2/a^2) \quad (6)$$

where

$$I_{max} = \frac{2P}{\pi(a/2)^2} = \frac{8P}{\pi a^2}$$

Furthermore, from Fig. 2 the power density from combustion, I_{comb}, can be expressed as

$$I_{comb} = \frac{\rho(V)(l)\Delta H}{\delta} = \frac{\rho l(2\alpha)(\Delta H)}{R\delta} \times s \quad \text{where } s = \frac{VR}{2\alpha} \quad (7)$$

Equation 5 can be expressed as

$$T_{mp} = T_{rm} + \frac{1}{2\pi lK(1-e^{-2})}\int_0^{a/2}\left(\frac{8P}{\pi a^2}\right) \times \exp\left(\frac{-8r^2}{a^2}\right) r\,dr \int_0^{2\pi} \exp(-Vr\cos\theta/2\alpha) \times K_0[V(R^2 - 2Rr\sin\theta + r^2)^{1/2}/2\alpha]d\theta + \frac{1}{2\pi lk}\int_R^{R+\delta/2}\left(\frac{\rho Vl(\Delta H)}{\delta}\right) r\,dr \times \int_{\pi/2}^{3\pi/2} \exp(-Vr\cos\theta/2\alpha) \times K_0[V(R^2 - 2Rr\sin\theta + r^2)^{1/2}/2\alpha]d\theta \quad (8)$$

The term $(1-e^{-2})$ was added to offset the difference between integrating from zero to infinity in the integral of laser power density.

By setting $r' = r/R$ and $s = VR/2\alpha$, Equation 8 becomes

$$T_{mp} = T_{rm} + \frac{R^2}{2\pi lK(1-e^{-2})}\int_0^{a/2R} A \times \left(\frac{8P}{\pi a^2}\right) \times \exp\left(\frac{-8R^2r'^2}{a^2}\right) r'dr' \int_0^{2\pi} \exp(-sr'\cos\theta) \times K_0[s(r'^2 - 2r'\sin\theta + 1)^{1/2}]d\theta + \frac{R^2}{2\pi lk}\int_1^{1+\delta/2R} \eta\left(\frac{2\alpha\rho l(\Delta H)s}{R\delta}\right) r'\,dr' \times \int_{\pi/2}^{3\pi/2} \exp(-sr'\cos\theta) \times K_0[s(r'^2 - 2r'\sin\theta + 1)^{1/2}d\theta \quad (9)$$

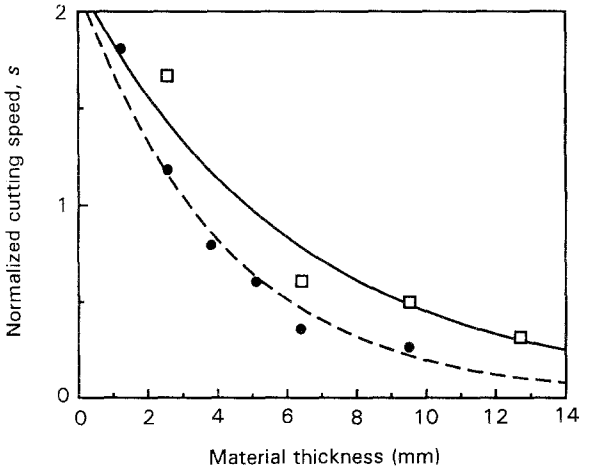

Figure 3 Cutting speed versus material thickness at various laser powers: (□) 1500 W, (●) 1000 W.

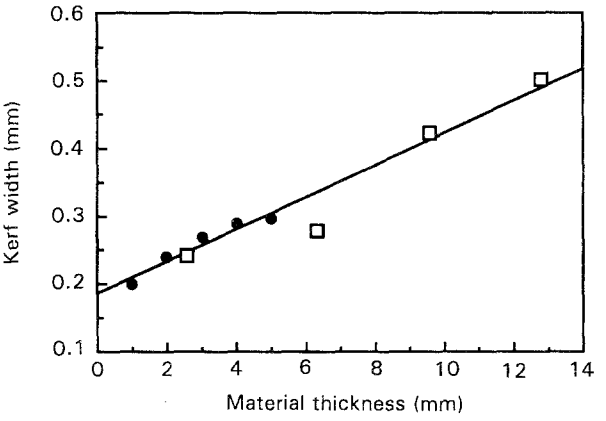

Figure 4 Kerf width versus material thickness in laser cutting: (□) present work, (●) after [26].

Here two constants, A and η, were added to Equation 9 to account for laser absorptivity and incomplete combustion inside the cutting kerf.

Again Equation 9 can be reduced to

$$T_{mp} = T_{rm} + \frac{A \times R^2}{2\pi lK(1-e^{-2})} I_{laser} + \frac{\eta \times R^2}{2\pi lK} I_{comb} \quad (10)$$

where I_{laser} corresponds to the first integral on the right-hand side of Equation 9 and I_{comb} the second.

4. Results and discussion

The experimental cutting speed versus workpiece thickness at two different laser power levels is plotted in Fig. 3 to within ± 10% accuracy. Fig. 4 shows a linear relationship between the kerf width and the section thickness. The reported values were taken as the average of the top and bottom kerf widths on the workpiece, both of which increased as the material thickness increased.

The thermal properties, such as thermal conductivity, K, and diffusivity, α, change with temperature. The values of the thermal properties at the average temperature (1000 K) between ambient and the melting point of steel are used in this work (Table I).

TABLE I Thermal properties of AISI 1020 steel at 1000 K

Meeting point, T_{mp} (K)	Density ρ ($kg\,m^{-3}$)	Thermal conductivity, k $W\,m^{-1}\,K^{-1}$	Thermal diffusivity, α ($m^2\,s^{-1}$)
1795	7877	31.3	3.42×10^{-6}

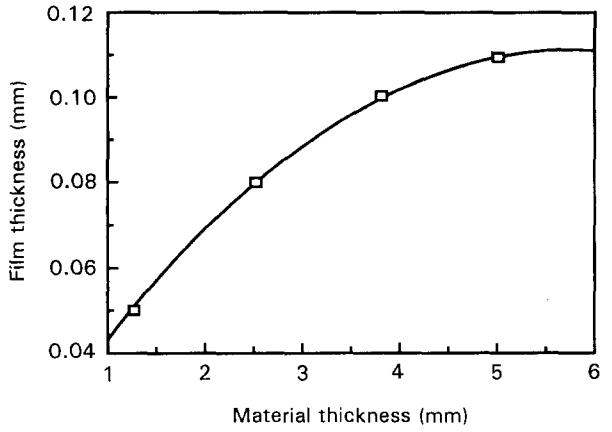

Figure 5 Relationship between average film thickness of liquid melt and material thickness in laser cutting (after Schuöcker [26]). Laser power, 1000 W; absorptivity, 75%.

The average thickness of the liquid melt film, δ, in the erosion cutting front has been studied by Schuöcker [26]. δ increases with workpiece thickness and is in the vicinity of 0.1 mm. Fig. 5 shows the average film thickness of liquid melt versus material thickness in laser cutting of steel at approximately 1 kW and 75% absorptivity [26]. These values were used in calculating the combustion power density in Equation 10. Roessler and Gregson [24] reported that the reflectivity of carbon steel subjected to 10.6 μm wavelength irradiation decreased significantly when peak power intensity exceeded $10^7\,W\,cm^{-2}$. Schuöcker [26] argued that the absorptivity of CO_2 laser in cutting steel should be about 80%. Hence, a laser absorptivity constant, A, equal to 0.8 was used in this model. Arata [27] reported that the oxidized product in the laser cutting of steel was FeO, which was confirmed by XRD analysis of combustion droplets. Ivarson *et al.* [16] concluded that 50% of iron in steel was oxidized to FeO in laser cutting and therefore $\eta = 50\%$ was used in the present model. Thus, the following combustion reaction occurs in laser cutting of carbon steels

$$Fe + \tfrac{1}{2}O_2 \rightarrow FeO \qquad \Delta H = 63.2\,Kcal\,mol^{-1}$$

I_{laser} and I_{comb} in Equation 10 were evaluated with a numerical method and were plotted as a function of s in Fig. 6a, b at various R values. Theoretical values of s and R can be solved by using Equation 10 and were plotted in Fig. 7. It can be seen that the model provides good agreement with experimentally obtained maximum cutting speed values. Also, the predicted values of kerf width agree well with experimental data in the medium thickness range (2–4 mm). Discrepancies between theory and experiment at $l = 1$ and 5 mm cases can be related to assumption (1) and (5). Heat loss due to evaporation in cutting thin-section material is significant and cannot be ignored. Therefore, the maximum cutting speed, as well as the temperature rise in Equation 4, and accordingly the kerf width will become smaller than those observed in practice. In cutting thicker sections, the temperature along the cutting depth (z direction) increases as the combustion reaction propagates and enlarges the kerf width. Under these circumstances, a three-dimensional model would be required to complete the analysis.

It is further found that the combustion energy (heat) is equal to approximately 55–70% of the total cutting energy (heat) in oxygen-assisted laser cutting of steel. This agrees with the previous report by Kamalu and Steen [3] who compared the laser cutting rates of steel with argon and oxygen assist gases and concluded that about 60% of the cutting energy is supplied by combustion.

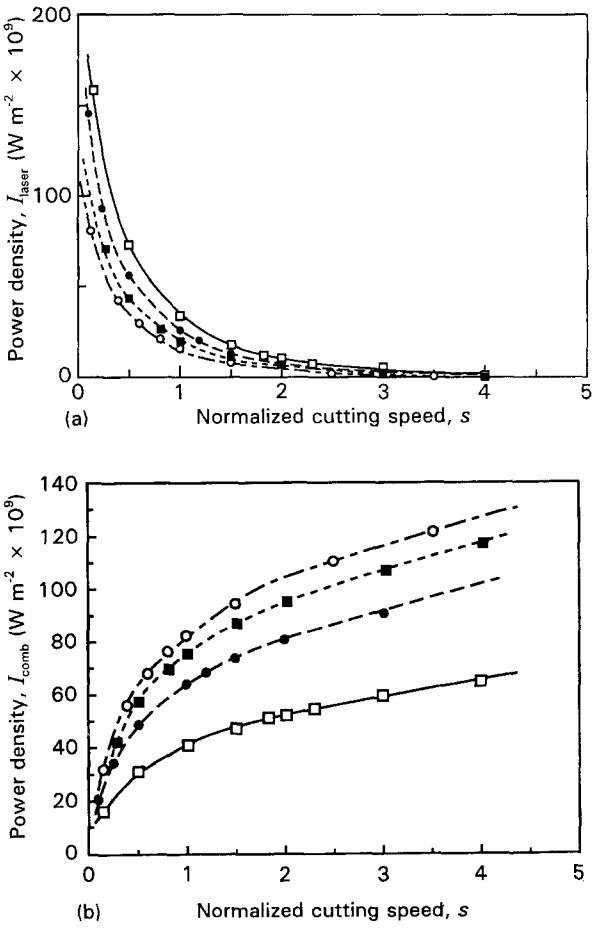

Figure 6 (a) I_{laser} versus s plot at various R values, and (b) I_{comb} versus s plot at various R values: Laser power, 1000 W. (□) $R = 0.105$ mm, (●) $R = 0.12$ mm, (■) $R = 0.135$ mm, (○) $R = 0.15$ mm.

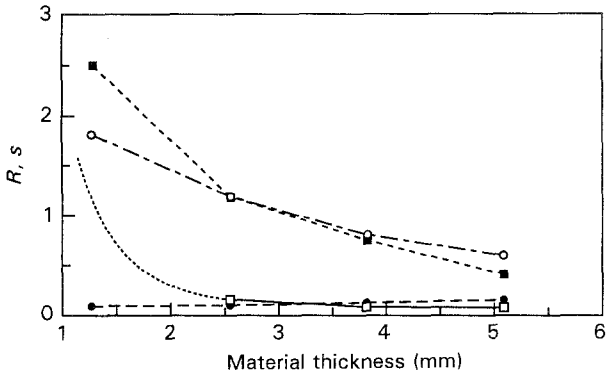

Figure 7 Theoretical and experimental maximum cutting speed, s and kerf width, R, versus material thickness. Laser power, 1000 W; absorptivity, 80%; combustion efficiency, 50%. (□) Theoretical R (mm), (●) experimental R (mm), (■) theoretical s, (○) experimental s.

5. Conclusions

The following conclusions are drawn based on these experimental and analytical studies of oxygen-assisted CO_2 laser cutting of carbon steel.

1. Experience and theoretical correlations between laser beam characteristics (power, absorptivity, mode pattern, focusability), combustion reaction (combustion efficiency, combustion heat) and material properties (thermal properties, density, thickness, liquid film thickness) were developed to predict accurately the processing parameters, such as the maximum cutting speed and kerf width for laser cutting of steel.

2. The cutting energy was supplied by the absorbed laser irradiation and the chemical reaction between steel and oxygen. The combustion effect was found to play a very important role in laser cutting. This energy can amount to about 55–70% of the total cutting energy as predicted and verified by this model.

Acknowledgements

The authors thank for the financial support from Iowa Department of Economic Development and National Science Foundation under contract DDM-9015658.

References

1. D. BELFORTE, in "The Laser Marketplace in 1988", Vol. 950 (Society of Photo Instrumentation Engineers) pp. 77–85.
2. J. F. READY, "Effects of High Power Laser Radiation" (Academic Press, New York, 1971).
3. J. N. KAMALU, and W. N. STEEN, in "Laser Materials Processings", edited by M. Bass (North-Holland Publishing Company, 1983) Chap. 2.
4. W. W. DULEY and J. N. GONSALVES, *Can. J. Phys.* **50** (1972) 215.
5. D. SCHUÖCKER and W. ABEL, in "Proceedings of Society of Photo Instrumentation Engineers" Sept. 1983 (Society of Photo Instrumentation Engineers, 1983) pp. 88–95.
6. D. SCHUÖCKER and B. WALTER, in Institute of Physics Conference Series No. 72 (Inst. Physics, 1984) pp. 111–116.
7. D. SCHUÖCKER, in "Proceedings of Society of Photo Instrumentation Engineers", Vol. 650 (Society of Photo Instrumentation Engineers, 1986) pp. 210–219.
8. M. F. MODEST and H. ABAKIANS, *ASME J. Heat Transfer* **108** (1986) 597.
9. G. CHRYSSOLOURIS, P. SHENG and W. C. CHOI, *Trans. ASME J. Engng Mater. Technol.* **112** (1990) 387.
10. G. CHRYSSOLOURIS, "Laser Machining Theory and Practice" (Springer-Verlag, New York, 1991).
11. H. ABAKIANS and M. F. MODEST, *ASME J. Heat Transfer* **100** (1988) 924.
12. S. Y. BAND and M. F. MODEST, *ibid.* **113** (1991) 663.
13. S. ROY and M. F. MODEST, *J. Thermophys. & Heat Transfer* **4** (1990) 199.
14. S. BIYIKLI and M. F. MODEST, *ASME J. Heat Transfer* **110** (1988) 529.
15. N. FORBES, in "Laser 1975 OptoElectronics Conference Proceedings", Munich, 1975.
16. A. IVARSON, J. POWELL and C. MAGNUSSON, *J. Laser Appns.* **3** (1991) 41.
17. D. BELFORTE, "Industrial Laser Annual Handbook" (Pennwell Books, Tulsa, OK, 1990).
18. K. A. BUNTING and G. CORNFIELD, *Trans. ASME J. Heat Transfer* (1973) 116.
19. V. P. BABENKO and P. TYCHINSKII, *Soviet J. Quantum Electronics* **2** (1973) 399.
20. Y. ARATA, and I. MIYAMOTO, *Trans. JWRI* **3** (1974) 1.
21. M. VICANEK and G. SIMON, *J. Appl. Phys.* **20** (1987) 1191.
22. J. F. READY, *ibid.* **36** (1965) 462.
23. S. CHARSCHAN, "Lasers in Industry", (Van Norstrand Reinhold, New York, 1972).
24. D. M. ROESSLER and V. G. GREGSON, *Appl. Opt.* **17** (1978) 992.
25. H. S. CARSLAW and J. C. JAEGER, "Conduction of Heat in Solids" (Clarendon Press, Oxford, 1959).
26. D. SCHUÖKER, in "Proceedings of Society of Photo Instrumentation Engineers", Vol. 952, (Society of Photo Instrumentation Engineers, 1988) pp. 592–599.
27. Y. ARATA, "Plasma, Electron and Laser Beam Technology" (American Society for Metals, Metals Park, OH, 1986) pp. 526–536.

Received 9 November 1993
and accepted 13 April 1994